Chinese Journal of Natural Medicines

# Xiaohuang Qudan decoction alleviates ANIT-induced cholestatic liver injury by inhibiting the JAK2/STAT3 pathway and regulating TH17/Treg

Zhangkui Tan, Lifeng Chen, Zhiqin Ye, Qiping Lu

**Citation:** Zhangkui Tan, Lifeng Chen, Zhiqin Ye, Qiping Lu, Xiaohuang Qudan decoction alleviates ANIT-induced cholestatic liver injury by inhibiting the JAK2/STAT3 pathway and regulating TH17/Treg, Chinese Journal of Natural Medicines, 2025, 23(4), 457-470. doi: 10.1016/S1875-5364(25)60854-5.

View online: https://doi.org/10.1016/S1875-5364(25)60854-5

Chinese Journal of Natural Medicines 23 (2025) 457-470

Contents lists available at ScienceDirect

Chinese Journal of Natural Medicines

journal homepage: www.cjnmcpu.com/

Original article

# Xiaohuang Qudan decoction alleviates ANIT-induced cholestatic liver injury by inhibiting the JAK2/STAT3 pathway and regulating TH17/Treg

Zhangkui Tan[a], Lifeng Chen[a], Zhiqin Ye[b], Qiping Lu[c,*]

[a] *Department of Rheumatology and Immunology, General Hospital of Central Theater Command of the People's Liberation Army, Wuhan 430070, China*
[b] *Department of Rheumatology, Hubei Provincial Hospital of Traditional Chinese Medicine, affiliated with Hubei University of Chinese Medicine, Wuhan 430061, China*
[c] *Department of General Surgery, General Hospital of Central Theater Command of the People's Liberation Army, Wuhan 430070, China*

ARTICLE INFO

*Article history:*
Received 23 January 2024
Revised 21 April 2024
Accepted 9 May 2024
Available online 20 April 2025

*Keywords:*
ANIT
TH17/Treg
Cholestatic liver injury
Xiaohuang Qudan decoction
JAK2/STAT3
UHPLC-MS/MS

ABSTRACT

Xiaohuang Qudan decoction (XHQDD) is a classical traditional Chinese medicine (TCM) formula widely used in the treatment of cholestatic liver injury. Despite its widespread use, the protective mechanism of XHQDD against cholestatic liver injury remains incompletely understood. The aim of this study was to investigate whether XHQDD mediates its beneficial effects by inhibiting the Janus kinase 2 (JAK2)/signal transducer and activator of transcription 3 (STAT3) pathway and regulating TH17/Treg balance. To this end, the researchers used Sprague-Dawley (SD) rats and established a cholestatic liver injury model by oral administration of alpha-naphthylisothiocyanate (ANIT). The experimental group was divided into six groups: Control (CON), ANIT, ursodeoxycholic acid (UDCA), XHQDD-low dose (XHQDD-L) group, XHQDD-medium dose (XHQDD-M) group, and XHQDD-high dose (XHQDD-H) groups. Then, after 7 d of treatment, various tests were performed to verify the results. Firstly, XHQDD and its drug-containing serum were analyzed by ultra-high performance liquid chromatography-mass spectrometry/mass spectrometry (UPLC-MS/MS), and 14 blood-entry components were identified. Then, bile flow was monitored and found to be significantly reduced in the model group, which was significantly reversed in the UDCA and XHQDD groups. To further assess ANIT-induced liver injury, hematoxylin and eosin (H&E) and Sirius red staining, alongside transmission electron microscopy (TEM), were employed to observe liver tissues, revealing hepatocellular injury, cholestasis, and hepatic fibrotic changes. Serum inflammatory factors and liver injury indicators were assessed using enzyme-linked immunosorbent assay (ELISA), indicating an inflammatory state in ANIT-induced liver injury rats. The expression levels of JAK2/STAT3-related genes and proteins in liver and intestinal tissues were measured *via* quantitative reverse transcription polymerase chain reaction (qRT-PCR), immunohistochemistry, immunofluorescence (IF) staining, and Western blottting (WB) assays. These studies revealed that the inflammatory state of liver-injured rats was inextricably linked to the inflammatory cascade associated with the JAK2/STAT3 pathway and that XHQDD may exert anti-inflammatory efficacy by inhibiting the JAK2/STAT3 pathway. Flow cytometry was used to determine the percentage of T helper 17 (Th17)/regulatory T (Treg) cells in serum and hepatocytes, and it was further found that XHQDD was able to regulate Th17/Treg immune homeostasis in liver-injured rats. The findings suggest that XHQDD markedly alleviates inflammation in ANIT rats, potentially treating cholestasis and liver injury through JAK2/STAT3 inhibition and Th17/Treg balance regulation.

## 1. Introduction

Cholestasis refers to a pathological condition characterized by impaired bile formation, secretion, and excretion. This impairment can arise from various factors, either intrinsic or extrinsic to the liver, leading to an inability of the bile stream to flow appropriately into the duodenum. Instead, bile may enter the bloodstream [1]. Cholestatic liver injury results from the accumulation of toxic bile acids (BAs), a consequence of bile stasis, thereby inducing further hepatic damage [2]. Clinically, patients may present with symptoms including itching, fatigue, yellowish urine, and jaundice. Notably, elevations in serum alkaline phosphatase (ALP) and gamma-glutamyl transferase (GGT) levels often emerge before the manifestation of these symptoms. Disease progression may lead to hyperbilirubinemia, which in severe cases can result in complications such as cirrhosis, liver failure, and death [3]. Hepatobiliary disorders primarily characterized by cholestasis, stemming from varied causes, are broadly termed cholestatic liver diseases. It is crucial to note that cholestasis can exacerbate liver damage.

* Corresponding author.
*E-mail address:* ptwklqp111@163.com

https://doi.org/10.1016/S1875-5364(25)60854-5

Cholestasis can be categorized into intrahepatic and extrahepatic forms, based on the specific site of impaired bile flow [4]. Intrahepatic cholestasis may stem from genetic or acquired factors, including mutations in genes encoding BA transport proteins, immune-mediated destruction of bile ducts, or drug-related mechanisms [5]. Conversely, extrahepatic cholestasis often involves a physical obstruction of bile flow within the liver or gallbladder, typically caused by gallstones or malignant growths [6]. The multifactorial nature of cholestasis renders it a complex condition to study, diagnose, and manage.

The pathophysiology of cholestatic liver injury involves complex interactions between liver cells, bile duct cells, immune cells, and intricate processes that regulate BA homeostasis [7]. Accumulation of BAs in liver cells leads to oxidative stress, inflammation, and activation of various signaling pathways, contributing to liver injury [8, 9]. Furthermore, the growing understanding of the immune system's role in cholestasis, particularly the balance between Th17 and Treg cell populations, highlights the potential of innovative immunotherapeutic approaches for managing cholestatic liver injury [10, 11]. In patients with primary biliary cholangitis (PBC), the frequency and absolute counts of Treg cells are significantly reduced, while the percentage and absolute counts of Th17 cells are elevated. Th17 and Treg cells play pivotal roles in the pathogenesis of PBC [12-14]. The Janus kinase 2 (JAK2)/signal transducer and activator of transcription 3 (STAT3) pathway has been identified as a crucial mechanism in cholestatic liver injury [15, 16]. Activation of the JAK2/STAT3 pathway in cholestatic patients exacerbates the pro-inflammatory effects [17].

The liver-gut axis is critical in cholestatic liver injury, a common feature of which is impaired BA excretion and/or enterohepatic circulation [18]. The enterohepatic circulation of BAs efficiently maintains BA homeostasis to prevent the accumulation of toxic BAs and to prevent liver inflammation and injury [19]. Interruption of the enterohepatic circulation of BAs prevents cholestatic liver and bile duct injury [20]. Current medications, including ursodeoxycholic acid and obeticholic acid, play a crucial role in managing cholestatic conditions, but they often display limited efficacy in severe cases [21].

Xiaohuang-Qudan decoction (XHQDD), a renowned herbal formula in Traditional Chinese Medicine (TCM) originating from "*Shishimilu* (The Secret Book of the Stone Chamber) " has a long history of treating liver and gallbladder ailments. The formula comprises five herbs. According to TCM principles, it is traditionally prescribed for tonifying the spleen, eliminating dampness, promoting bile secretion, and alleviating jaundice. Artemisiae Scopariae Herba (Yin-chen) is a commonly used drug for the treatment of cholestatic diseases. Its pharmacological effects mainly include hepatoprotective and choleretic properties [22, 23]. It has been found that Artemisiae Scopariae Herba can improve cholestasis by inhibiting the inflammatory factor pathway [24]. Plantaginis Semen (Che-qian-zi), Coicis Semen (Yi-yi-ren), and Poria (Fu-ling) have the effect of strengthening the spleen and inducing dampness in Chinese medicine, and modern research has shown that their diuretic effect is consistent with the need to "remove dampness" in the treatment of jaundice in Chinese medicine [25]. Cinnamomi Cortex (Rou-gui) is mainly used as a medicinal guide in the formula, so that the heat of the liver and gallbladder can be discharged from the urine. The above four herbs have anti-inflammatory [26-29] and immunomodulatory effects [30-32] in modern pharmacological studies. In clinical settings, XHQDD has demonstrated efficacy in mitigating a range of hepatobiliary conditions, encompassing acute and chronic hepatitis, jaundice, and cholestasis[33]. Despite its traditional use, contemporary pharmacological research focusing on the hepatoprotective capabilities of XHQDD remains scant. The specific mechanisms underpinning its hepatoprotective effects, especially in relation to cholestasis, are yet to be thoroughly explored and understood. In this study, our objective is twofold: first, to assess the protective influence of XHQDD on alpha-naphthylisothiocyanate (ANIT)-induced intrahepatic cholestasis in rats, and second, to unravel its potential therapeutic mechanisms. For the latter, we employ a multifaceted approach, leveraging Serum Pharmaceutical Chemistry, the JAK2/STAT3 pathway, and the Th17/Treg immune balance.

## 2. Material and Methods

### *2.1. Chemicals and reagents*

ANIT (N4525), Hematoxylin (H9627), Eosin Y (E4009), and Direct Red 80 (365548) were obtained from Sigma-Aldrich (Milwaukee, USA). Ursodeoxycholic acid (UDCA, H20181059) was procured from Losan Pharma GmbH (Freiburg, Germany). Enzyme-lin-linked immunosorbent assay (ELISA) kits for rat interleukin (IL)-6 (MM-0190R2), IL-17 (MM-0088R2), IL-10 (MM-0195R2), IL-23 (MM-0414R2), transforming growth factor (TGF)-β (MM-20594R2), and tumor necrosis factor (TNF)-α (MM-0180R2) were sourced from Jiangsu Meimian Industrial Co. (Yancheng, China). Assay kits for ALP (C003-b), alanine alanine transaminase (ALT, C001-a), aspartate aminotransferase (AST, C002-a), and gamma-glutamyltransferase (*γ*-GT, C009-b) were purchased from Changchun Huili Biotech Co., Ltd. (Changchun, China). Total bilirubin (TBIL, C019-1), direct bilirubin (DBIL, C019-2), and total bile acid (TBA, E003-2) kits were obtained from Nanjing Jiancheng Bioengineering Institute (Nanjing, China). Phosphorylated STAT3 (p-STAT3) monoclonal antibody (Tyr705, 9145S) and total STAT3 monoclonal antibody (124H6, 9139S) were acquired from Cell Signaling Technology (Danfoss, USA). Antibodies against phosphorylated JAK2 (p-JAK2, Tyr931) (AF3024), JAK2 (AF6022), forkhead box P3 (Foxp3) (AF6544), retinoic acid-related orphan receptor gamma t (RORγt) (DF3196), *α*-smooth muscle actin (*α*-SMA) (AF1032) and Collagen I (Col I) (AF7001) were procured from Affinity Bioscience Ltd. (Changzhou, China). Glyceraldehyde-3-phosphate dehydrogenase (GAPDH, AB-P-R001)) was sourced from Hangzhou Goodhere Biotechnology Co., Ltd. (Hangzhou, China). CD3 monoclonal antibody (MA5-16763), CD4 monoclonal antibody (11-0040-81) and IL-17A monoclonal antibody (12-7177-81) were procured from Thermo Scientific (Waltham, USA). Foxp3 antibody (320007) and CD25 antibody (202113) were obtained from BioLegend (San Diego, USA).

### *2.2. Preparation of XHQDD*

The XHQDD is composed of five Chinese medicinal herbs, all sourced from the General Hospital of the Central Theater Command (Wuhan, Hubei): Artemisiae Scopariae Herba, Coicis Semen, Poria, Plantaginis Semen, and Cinnamomi Cortex. These five herbal components were mixed in a ratio of 1∶9∶3∶9∶0.2, respectively (Supplementary Table 1). The herbs were authenticated by Prof. Chunhui Tao of Hubei University of Chinese Medicine. The traditional decoction method was employed to prepare the XHQDD. First, the herbs were combined and soaked in water, with the volume of water being six times the weight of the herbs, for 1.5 h. Subsequently, the herbs were decocted for 1 h, initially on a high flame and then on a low flame. The dregs were then separated and discarded, and the remaining liquid was collected. This process was repeated, and the resulting filtrates were combined. The combined liquid was then concentrated using a rotary evaporator, yielding a final drug mass concentration of 0.66 $g \cdot mL^{-1}$, based on the weight of the raw ingredients. Finally, the concentrated decoction was stored in a refrigerator at 4 °C for future use.

### 2.3. Preparation of XHQDD medicated serum

Twenty male Sprague-Dawley (SD) rats (6 weeks old, weighing 210 ± 10 g) were randomly assigned to two groups. The dosage of the XHQDD crude drug was determined using the rat-to-human dosage relationship, calculated as follows: crude drug dosage per kilogram of rats = adult drug dosage (g)/adult body weight × 6.3. Rats in the XHQDD group received an oral administration of XHQDD decoction (11.23 $g \cdot kg^{-1} \cdot d^{-1}$) twice daily for 5 d, while rats in the control (CON) group received an equivalent volume of saline, twice daily for 5 d. The rats were fasted for 12 h before being sacrificed. Two hours after the final dose, the rats were anesthetized with sodium pentobarbital (50 $mg \cdot kg^{-1}$), and their blood was collected and centrifuged at 3000 $r \cdot min^{-1}$ for 15 min at 4 °C to separate serum. The serum samples were stored at −80 °C for subsequent analysis.

### 2.4. Ultra-high performance liquid chromatography-tandem mass spectrometry (UHPLC-MS/MS) analysis

The components of the XHQDD water extract were analyzed and identified by UHPLC-MS/MS. The XHQDD water extract was dissolved in an 80% methanol–water solution and centrifuged at 12 000 $r \cdot min^{-1}$ for 15 min at 4 °C. The supernatant was applied to UHPLC-MS/MS analysis. XHQDD was performed on a UHPLC system (Vanquish, Thermo Fisher Scientific) with a Waters UPLC BEH $C_{18}$ column (1.7 μm, 2.1 mm × 100 mm). The flow rate was set at 0.5 $mL \cdot min^{-1}$, and the sample injection volume was 5 μL. The mobile phase consisted of 0.1% formic acid in water (A) and 0.1% formic acid in acetonitrile (B). The elution gradient program was as follows: 0–11 min, 85%–25% A; 11–12 min, 25%–2% A; 12–14 min, 2% A; 14–14.1 min, 2%–85% A; 14.1–16 min, 85% A. An Orbitrap Exploris 120 mass spectrometer coupled with Xcalibur software was used to acquire the MS and MS/MS data in information-dependent acquisition (IDA) mode. The mass range scanned was from *m/z* 100 to 1500, and the top four ions from each cycle were selected for further MS/MS analysis. The instrumental parameters were as follows: sheath gas flow rate, 35 arbitrary units; auxiliary gas flow rate, 15 arbitrary units; ion transfer tube temperature, 350 °C; vaporizer temperature, 350 °C; full MS resolution, 60 000; MS/MS resolution, 15 000; collision energy, 16/32/48 in normalized collision energy (NCE) mode; spray voltage, +4 kV (positive) or −3.8 kV (negative). The raw data from the mass spectrometry analysis were processed using XCMS software, which included retention time correction, peak identification, peak extraction, peak integration, and peak alignment. The peak information of the compounds was then searched against an in-house secondary mass spectrometry database provided by Shanghai BIOTREE Biotech Co., Ltd..

### 2.5. Animals and treatment

Sixty male SD rats (6 weeks old, weighing 210 ± 10 g) were used in this study, which were purchased from Liaoning Changsheng Biotechnology Co., Ltd. (Liaoning, China), License number: SCXK 2020-0001. The rats were acclimated for five days to the controlled environment (23 ± 1 °C, 30%–40% relative humidity) with unrestricted access to food and water. All animal procedures were conducted in accordance with the National Institutes of Health Guidelines for the Use of Laboratory Animals and approved by the Animal Ethics Committee of Wuhan Myhalic Biotechnology Co., Ltd. (No. HLK-20230415-001).

This study was conducted in strict accordance with the recommendations of the Guidelines for the Care and Use of Laboratory Animals of the Ministry of Science and Technology of China. The rats were randomly divided into six groups of 10: Con group, ANIT group, UDCA group, XHQDD-low dose (XHQDD-L) group, XHQDD-medium dose (XHQDD-M) group, and XHQDD-high dose (XHQDD-H) group. Each rat in the Con group was given normal saline for seven consecutive days, and, on the fifth day was given the vehicle (olive oil) alone. The ANIT group was treated with normal saline for seven days and received a separate administration of 60 $mg \cdot kg^{-1}$ ANIT (dissolved in olive oil) on the fifth day. The UDCA group was treated with UDCA at a dosage of 60 $mg \cdot kg^{-1}$ each day for 7 d, and was administered with 60 $mg \cdot kg^{-1}$ ANIT on the fifth [34-36]. The XHQDD (L, M, H) groups were given intragastric administrations of XHQDD at doses of 5.62, 11.23, and 22.47 $g \cdot kg^{-1} \cdot d^{-1}$, respectively for seven consecutive days. On the fifth day, the rats in the XHQDD groups received 60 $mg \cdot kg^{-1}$ ANIT (Fig. 1 A). The dosage of the XHQDD crude drug was calculated using the rat-to-human dosage relationship based on the following conversion formula: crude drug dosage per kilogram of rats = adult drug dosage (g)/adult body weight × 6.3. The dosage of the XHQDD-M was determined from the clinical application dosages [37]. The dosage of the XHQDD-L was half of the XHQDD-M, and the dosage of the XHQDD-H was twice that of the XHQDD-M.

### 2.6. Determination of bile flow rate

Rats were anesthetized *via* an intraperitoneal injection of sodium pentobarbital at a dosage of 50 $mg \cdot kg^{-1}$. Within a sterile environment, the liver was exposed, and the common bile duct was separated. A polyethylene tube was inserted into the common bile duct to facilitate bile collection. Following the administration, bile fractions were gathered at 15-minute intervals, spanning from −15 to 0, 0 to 15, 15 to 30, 30 to 45, 45 to 60, 60 to 75, and 75 to 90 min.

### 2.7. ELISA and biochemical analyses

The levels of the inflammatory factors IL-6, IL-17, IL-10, IL-23, TGF-β, and TNF-α in the serum supernatant were determined using ELISA kits, following the manufacturer's instructions. Serum biochemical parameters, including AST, ALT, ALP, TBIL, DBIL, TBAs, and γ-GT, were measured using an automatic biochemical analyzer (Chemray 240, Shenzhen, China).

### 2.8. Histopathologic evaluation

The liver tissue was sectioned into small pieces measuring 0.5 cm × 0.5 cm and completely fixed with a 4% paraformaldehyde solution. The samples underwent routine dehydration and paraffin embedding. Sections from each sample were cut, and histopathological analysis was performed using hematoxylin and eosin (H&E) staining as well as Sirius red staining.

### 2.9. Immunofluorescence (IF) assay

The liver tissue samples were fixed with 4% paraformaldehyde, dehydrated, cleared, embedded in paraffin, sectioned, and baked. The sections were then dewaxed and underwent antigen retrieval. The sections were incubated with goat serum for 30 min to block nonspecific binding. Primary antibodies against IL-10 and IL-17 (1∶100 dilution) were added and incubated overnight (15 h) at 4 °C. Subsequently, the sections were incubated with CY3-labeled goat anti-rabbit IgG secondary antibody (1∶100 dilution) for 1 h. Finally, the cells were counterstained with DAPI and observed under a fluorescence microscope. The results of the immunofluorescence analysis were quantified using ImageJ software.

### 2.10. Quantitative reverse transcription polymerase chain reaction (qRT-PCR) assay

QRT-PCR was applied to determine the effect of XHQDD on

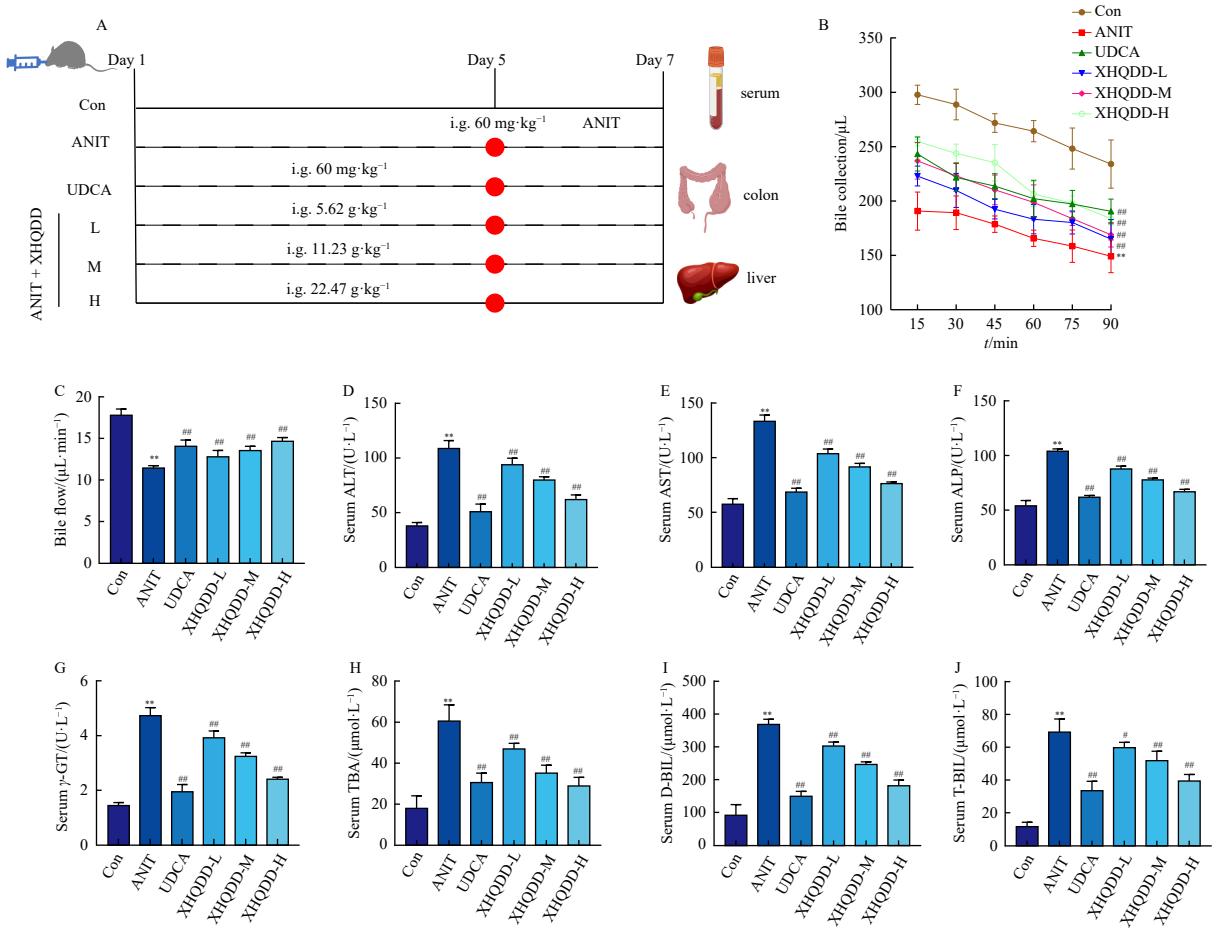


**Fig. 1** XHQDD attenuates ANIT-induced cholestatic liver injury *in vivo*. (A) Experimental design protocol. (B–C) 90-Minute bile flow monitoring. (D–J) Serum levels of ALT (D), AST (E), ALP (F), γ-GT (G), TBA (H), D-BIL (I) and T-BIL (J). Data are shown as means ± SD ($n$ = 10). $^{**}P < 0.01$ *vs* Con group; $^{\#}P < 0.05$, $^{\#\#}P < 0.01$ *vs* ANIT group

*JAK2*, *STAT3*, *Foxp3,* and *RORγt* expressions in liver tissues. Total RNA was isolated using Trizol reagent (Invitrogen) and reverse-transcribed into complementary DNA (cDNA). Real-time PCR was then performed using SYBR Green Master Mix and the specific primers listed in Supplementary Table 2. The expression levels were normalized to the GAPDH control.

### 2.11. Western blotting (WB) assay

Frozen liver and colon tissues were cut into small pieces and homogenized in RIPA protein lysis buffer. The homogenate was placed on ice for 30 min, vortexed 3 times, and centrifuged at 12 000 r·min$^{-1}$ for 5 min at 4 °C. The supernatant was then collected and the protein concentration was measured with a BCA protein assay kit. Proteins were separated by SDS-PAGE, transferred to a PVDF membrane, and immunoblotted. The membranes were blocked in 5% skim milk for 1 h and washed three times with PBST for 15 min each. The blotted membranes were incubated with primary antibodies against JAK2, p-JAK2, STAT3, p-STAT3, Foxp3, RORγt, and GAPDH (dilution ratio = 1∶1000) overnight at 4 °C. PVDF membranes were washed 5 times with PBST for 5 min each and incubated with secondary antibody (1∶5000) for 2 h. Protein blots were visualized using an electrochemiluminescence assay. JAK2, p-JAK2, STAT3, p-STAT3, Foxp3, and RORγt were analyzed, and GAPDH was used as a reference standard for the amount of samples loaded.

### 2.12. Immunohistochemistry (IHC)

Colon tissue sections were collected for IHC to determine the expression levels of p-JAK2 and p-STAT3. The tissue samples underwent a series of processing steps, including dehydration, paraffin embedding, sectioning, and deparaffinization, followed by antigen retrieval. Endogenous peroxidase activity was blocked using 3% hydrogen peroxide, and the sections were incubated with goat serum to prevent nonspecific binding. The sections were then incubated with primary antibodies targeting p-JAK2 and p-STAT3 overnight at 4 °C. Subsequently, the sections were incubated with a horseradish peroxidase (HRP)-conjugated secondary antibody against rabbit at 37 °C for 30 min. Visualization was achieved using 3,3'-diaminobenzidine (DAB) as the chromogen, and the sections were counterstained with Mayer's hematoxylin. Positive expression, indicated by tan-colored particles, was observed under an inverted microscope at 400× magnification. The immunohistochemical staining in the tissue samples was quantified using ImageJ software.

### 2.13. Flow cytometry analysis

Non-parenchymal liver cells and peripheral blood lymphocytes were isolated. Then, the cells were centrifuged and resuspended in phosphate-buffered saline (PBS). After centrifugation and two washes, phorbol 12-myristate 13-acetate (PMA) at a final concentration of 25 ng·mL$^{-1}$, ionomycin at a final concentration of 1 μg·mL$^{-1}$, and brefeldin A at a final concentration of 10 ng·mL$^{-1}$ were added, and the cells were incubated at 37 °C for 4 h. Subsequently, the following antibodies were added according to the experimental requirements: CD3 (10 μL/test), CD4 (0.5 μg/test), and CD25 (5 μL/test), and the cells were incubated for 30 min at 4 °C in the dark. After centrifugation and washing the cells with PBS, 1 mL of membrane-breaking reagent was added, and the cells were incubated in the dark for 50 min. Then, 1 mL of

washing reagent was added, and the cells were centrifuged at 2000 r·min$^{-1}$ for 5 min. Antibodies against IL-17A (0.5 μg/test) and Foxp3 (10 μL/test) were added as required for the experiment. Finally, the cells were centrifuged and resuspended in PBS, and the data were analyzed using a flow analyzer.

### 2.14. Statistical analysis

The data were expressed as mean ± standard deviation (SD) and were analyzed using SPSS 20.0 software. When the data followed a normal distribution and had equal variances, a one-way analysis of variance (ANOVA) was employed, followed by Tukey's post hoc analysis. Alternatively, the Kruskal-Wallis test was utilized. The threshold for statistical significance was set at $P < 0.05$. Graphs were produced using GraphPad Prism 8 (GraphPad, San Diego, CA, USA) was used to generate the graphs.

## 3. Results

### 3.1. Compounds identified in XHQDD and medicated serums

Using an untargeted LC-MS/MS detection and analysis technique, we identified the chemical constituents of XHQDD drugs and rat serum infused with these drugs. We employed the Orbitrap platform with both positive ion (POS) and negative ion (NEG) modes. By setting the composite score threshold at > 0. 6, we discovered a total of 669 compounds in XHQDD (Supplementary material Figs. 1A and 1B). A total of 14 herbal prototype compounds were detected in rat drug-containing serum including nicotinic acid, uracil, 1-isothiocyanato-9-(methylsulfinyl)-nonane, choline, 3-*O*-*C*affeoyl-4-*O*-methylquinic acid, 1,7-dimethyl-7-(4-methyl-3-penten-1-yl)bicyclo[2.2.1]heptan-2-ol, ganoderic acid DM, *ent*-16α-hydroxy-17-acetoxy-19-kauranal, (*S*)-11,12,13-trinor-7-calamenone, sugiol, petroselinic acid, 3,8α-dihydroxy-5-isopropylidene-3,8-dimethyl-2,3,3α,4,5,8α-hexahydro-6(1*H*)-azulenone, curdione and kukoamine A (Supplementary material Figs. 1C and 1D, Supplementary material Table 3).

### 3.2. XHQDD improves bile flow and liver injury

Bile flow is a critical index of intrahepatic cholestasis induced by ANIT. As shown in Figs. 1 B and 1C, the bile flow in ANIT-induced intrahepatic cholestasis rats decreased significantly ($P < 0.01$) when compared with that of the normal group. After treatment with XHQDD and UDCA, the bile flow of ANIT-induced intrahepatic cholestasis rats significantly increased in the XHQDD (L, M, H) group ($P < 0.01$) and the UDCA group ($P < 0.01$), respectively.

As previously reported [38, 39], serum ALT, AST, ALP, and γ-GT levels were significantly higher in ANIT-induced cholestatic rats compared to that of Con rats. However, treatment with XHQDD effectively reduced these liver damage indices ($P < 0.01$, Figs. 1D–1G). Serum TBIL, DBIL, and TBA are crucial biomarkers of cholestasis. ANIT administration markedly increased serum DBIL, TBIL, and TBA levels, whereas XHQDD treatment resulted in a significant reduction in these bile markers in the cholestatic rats ($P < 0.01$, Figs. 1 H–1J).

### 3.3. XHQDD alleviates liver pathological injury and liver fibrosis in ANIT rats

Histological assessments of the liver further indicated ANIT-induced hepatotoxicity. Liver tissue in the Con group exhibited normal structure and did not demonstrate any abnormal morphological changes (Fig. 2A). In contrast, the ANIT groups displayed greater lipid deposition, increased hepatocyte nuclear pyknosis, enlargement of connective tissue around the cells, and bile duct hyperplasia with inflammatory cell infiltration in the portal area (Fig. 2B). Comparatively, the pathological changes in the UDCA group showed marked improvement, with reduced hepatic cell necrosis and inflammatory infiltration, and morphology and structure close to normal (Fig. 2C). The liver tissue in the XHQDD-L group exhibited slight improvement compared to the model group (Fig. 2D). Similar to the UDCA group, most of the hepatic cells in the XHQDD-M and XHQDD-H group showed relatively normal morphology and structure (Figs. 2E and 2F), indicating a dose-dependent therapeutic effect of XHQDD. To evaluate the severity of liver fibrosis, collagens in liver tissues were examined by Sirius Red staining. The ANIT group displayed increased collagen deposition, marked steatosis, and hepatocyte ballooning compared to the Con group (Figs. 3A and 3B). IHC further revealed higher expressions of α-SMA and Col I proteins in the ANIT group compared to the Con group. The mean integrated optical density (IOD) values indicated that XHQDD decreased the expression of α-SMA and Col I proteins in a dose-dependent manner ($P < 0.01$, Figs. 3C–3F). This phenomenon was reversed after treatment with UDCA and XHQDD, with the effect being more pronounced in the XHQDD-H group (Figs. 3A–3F). These results indicate that XHQDD administration mitigates ANIT-induced liver fibrosis in rats.

Moreover, we also observed microstructural changes in the liver by transmission electron microscopy (TEM). The Con group showed a normal structure, abundant organelles, and a clear structure (Fig. 4A). As shown in Fig. 4B, hepatocytes in the ANIT group exhibited disordered cellular organelles, nuclear chromatin aggregation, irregular nuclei, swollen mitochondria, and vacuolated cytoplasm. However, these changes were reversed after treatment with XHQDD and UDCA. Interestingly, the study also identified the presence of autophagy in liver cells during the course of XHQDD and UDCA treatment. These findings align with previous research (Figs. 4C–4F).

### 3.4. XHQDD inhibits the JAK2/STAT3 pathway and improves liver inflammation in ANIT rats

Inflammatory cytokines play pivotal roles in the pathogenesis of cholestatic liver injury and represent significant therapeutic targets in both human and animal models of these diseases. To assess the impact of ANIT on systemic inflammatory cytokines, this study examined the circulating levels of pro-inflammatory and anti-inflammatory cytokines. The serum levels of pro-inflammatory cytokines, including IL-6, IL-17A, IL-23, TGF-β, and TNF-α, were significantly increased in the ANIT group compared with those in the Con group. In contrast, treatment with XHQDD and UDCA significantly reduced the levels of these pro-inflammatory cytokines ($P < 0.01$, Figs. 5A and 5C–5F). Conversely, the serum level of the anti-inflammatory cytokine IL-10 was significantly decreased in the ANIT group compared to the Con group, and XHQDD and UDCA treatment markedly increased the level of IL-10 ($P < 0.01$, Fig. 5B). These results indicate that XHQDD and UDCA can effectively reduce the levels of pro-inflammatory cytokines and increase the level of an anti-inflammatory cytokine, suggesting their potential therapeutic benefits in the management of cholestatic liver injury.

To explore the mechanism by which XHQDD inhibits the liver inflammatory response in the rat ANIT-induced cholestatic liver injury model, we evaluated the mRNA expression of JAK2 and STAT3, as well as the protein levels of JAK2, p-JAK2, STAT3, and p-STAT3 in liver tissues, using qRT-PCR and WB assays. In liver tissues, JAK2 and *STAT3* mRNA levels in the ANIT group were higher than those in the Con group. XHQDD and UDCA inhibited the expressions of JAK2 and *STAT3* mRNA significantly ($P < 0.01$,

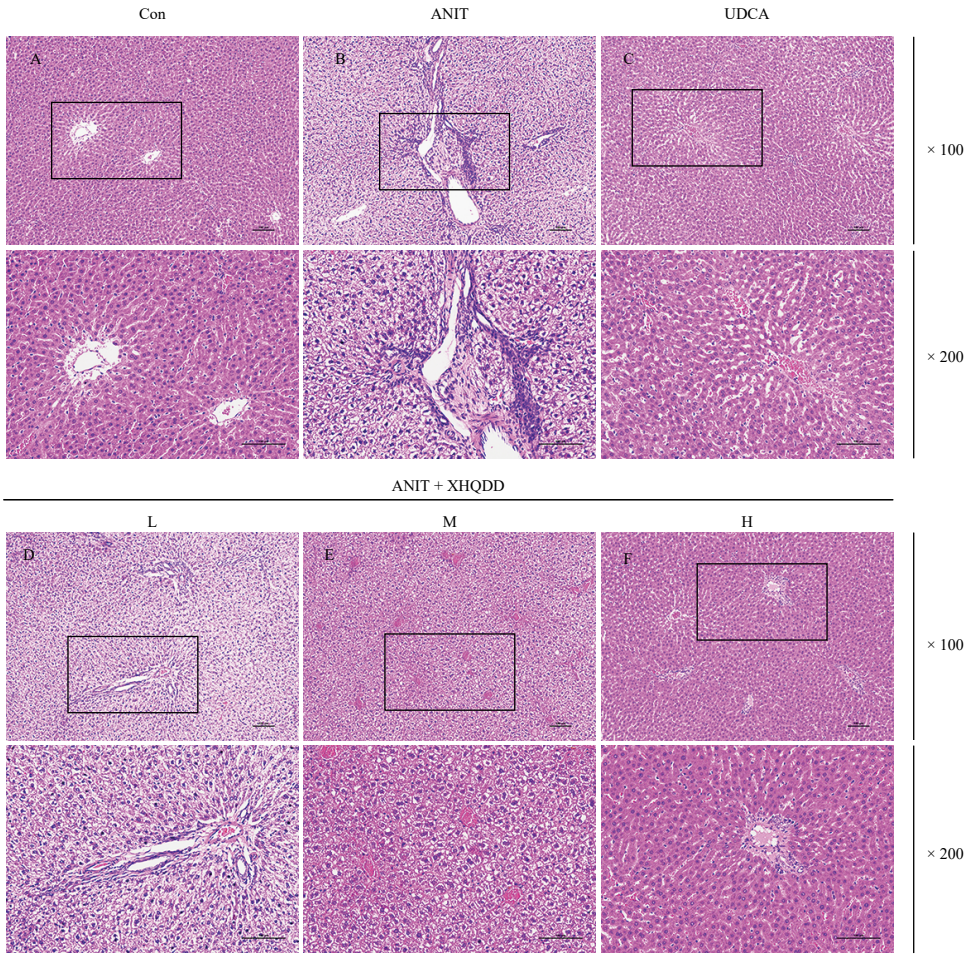


**Fig. 2** HE stained liver sections. Observed at 100× and 200×, respectively. Scale bar = 100 μm.

Figs. 5G and 5H). The WB results also showed that XHQDD and UDCA reduced the protein levels of p-JAK2 and p-STAT3 ($P < 0.01$), while the total protein levels of JAK2 and STAT3 were not changed ($P > 0.05$, Figs. 5 I and 5J). Furthermore, XHQDD reduced the levels of p-JAK2 and p-STAT3 proteins in a dose-dependent manner (Figs. 5K–5M). Based on these findings, we speculate that XHQDD may reduce the inflammatory response of the liver by inhibiting the activation of the JAK2/STAT3 signaling pathway.

IF analysis was employed to evaluate the expressions of IL-10 and IL-17 in each liver tissue sample (Figs. 6A and 6B). The results showed that the expression of IL-10 was significantly decreased, and the expression of IL-17 increased in the ANIT group compared with those in the Con group ($P < 0.01$). Furthermore, the data revealed that XHQDD and UDCA could reverse this observed phenomenon (Figs. 6C and 6D).

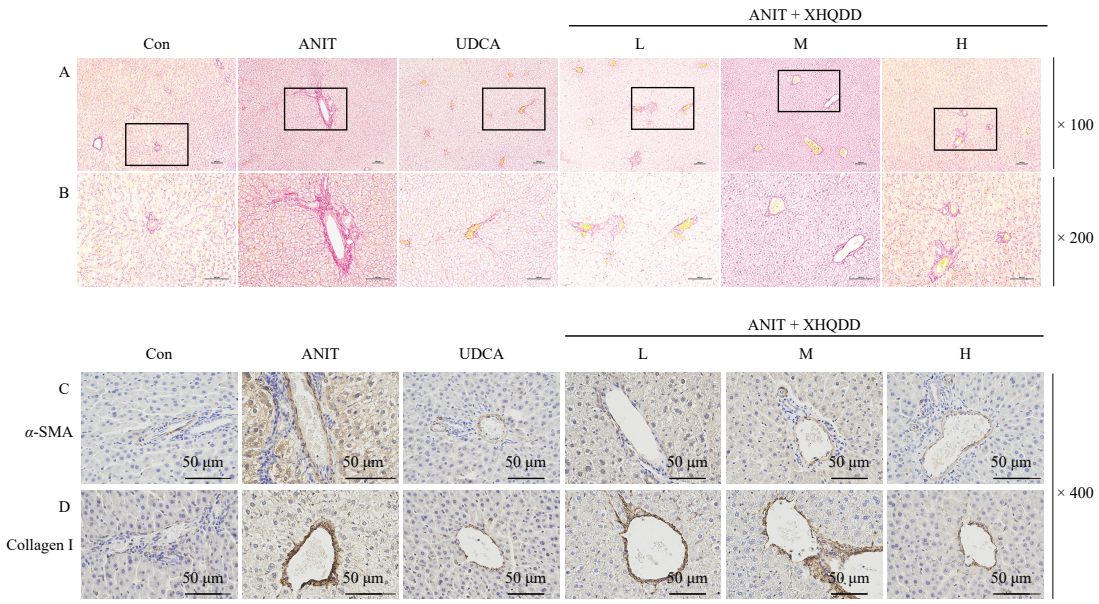

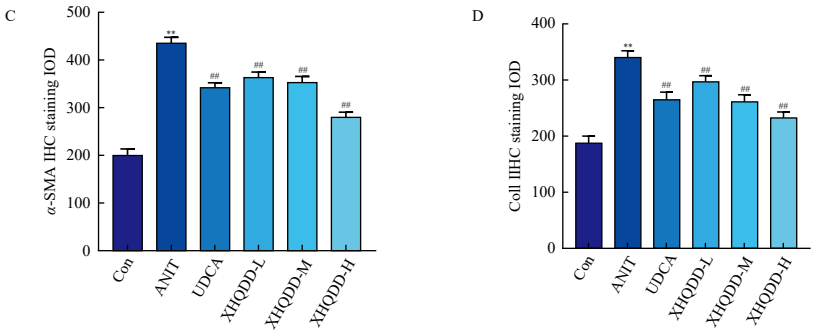


**Fig. 3** XHQDD improves hepatic fibrosis manifestations in ANIT rats. (A–B) Sirius red-stained liver sections. Observed at 100× and 200×, respectively. Scale bar = 100 μm. (C–D)Representative images of α-SMA and Collagen I protein expression in liver tissues were obtained using IHC (50 μm). (E–F) The results show the mean IOD of α-SMA and Collagen I proteins stained by IHC. Data are shown as means ± SD ($n$ = 10). $^{**}P < 0.01$ *vs* Con group; $^{\#\#}P < 0.01$ *vs* ANIT group.

### *3.5. XHQDD inhibits JAK2/STAT3 pathway in liver tissues*

The role of the liver-gut axis in liver diseases is widely acknowledged and has recently garnered significant research interest [40, 41]. BAs regulate intestinal immunity and enhance liver-gut circulation [42]. Consequently, we conducted a study to investigate the impact of XHQDD on the intestine in cholestatic liver injury, carrying out immunohistochemical analysis of p-JAK2 and p-STAT3 in colon tissues. The findings indicate that p-JAK2 and p-STAT3 protein expression was higher in the ANIT group compared to the Con group. The average integrated optical density (IOD) values indicate that XHQDD reduces the quantities of p-JAK2 and p-STAT3 proteins in a dose-dependent manner ($P$ < 0.01, Figs. 7A–7D). The aforementioned trend was also identified in p-JAK2 and p-STAT3 proteins by WB ($P$ < 0.01, Figs. 7G–7I). Furthermore, the transcription factor RORγt was notably increased in the ANIT cohort, while Foxp3 was significantly decreased, compared to the Con cohort. This pattern was then reversed by XHQDD in a dose-dependent manner ($P$ < 0.01, Figs. 7E–7G).

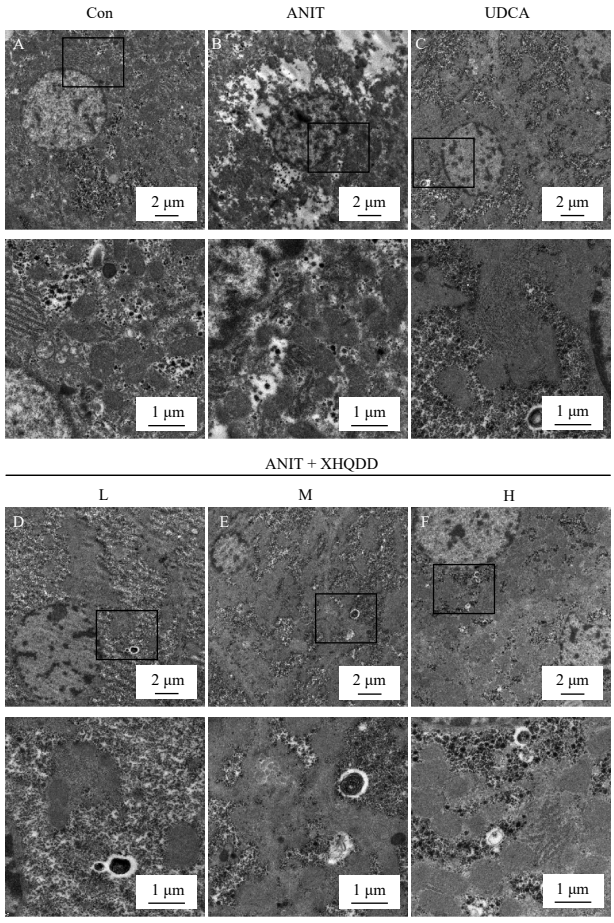


**Fig. 4** Transmission electron microscopy observation of liver ultrastructure. Scale bar = 1 μm

### *3.6. XHQDD rescued Th17/Treg imbalance in serum and liver*

This study aimed to determine if the XHQDD treatment had beneficial effects linked to the equilibrium of Th17 and Treg cells. The methodology involved measuring the percentages of Th17 cells ($CD4^+IL\text{-}17A^+$) and Treg cells ($CD4^+CD25^+Foxp3^+$) in the CD4 population of liver and serum using flow cytometry. The findings demonstrated a significant increase in the percentage of Th17 cells and a decrease in the percentage of Treg cells in both liver and serum in the ANIT group compared to the Con group ($P$ < 0.01). The Th17/Treg ratio showed the same trend. Interestingly, treatment with XHQDD and UDCA mitigated this alteration ($P$ < 0.01, Figs. 8A–8C, Figs. 9A–9E). The treatment effect of the UDCA group was significantly better than that of the low-dose XHQDD group, although UDCA and high doses of XHQDD exhibited comparable treatment effects.

The hepatic mRNA and protein expression levels of RORγt and FoxP3 were scrutinized through qRT-PCR and WB analysis. The findings demonstrated that RORγt mRNA and protein levels were markedly increased in the ANIT group compared to the control group (Figs. 8D, 8E, and 8H). In contrast, FoxP3 mRNA and protein levels were significantly downregulated (Figs. 8D, 8F, and 8G). Following treatment with XHQDD and UDCA, reductions in mRNA and protein levels of RORγt were observed, while expressions of *FoxP3* mRNA and protein levels were enhanced in ANIT rats ($P$ < 0.01, $P$ < 0.05). However, there was no significant difference in mRNA and protein expression levels of FoxP3, as well as *RORγt* mRNA expressions, between the XHQDD-L group and the ANIT group ($P$ > 0.05).

## 4. Discussion

TCM, which is mainly characterized by holistic concepts and evidence-based treatment, has accumulated rich experience in cholestatic liver injury and embodies great therapeutic potentials [43, 44]. XHQDD is a classic TCM formula for the treatment of jaundice, and its pharmacological mechanism has not been previously studied. This study employs low, medium, and high doses of XHQDD groups to investigate its mechanism in cholestatic liver injury treatment. The chemical composition of compound Chinese medicines forms the foundation of their efficacy. Analyzing the chemical and serum composition of Chinese medicine compounds aims to uncover their active ingredients and mechanisms of action, holding significant implications for the application and promotion of TCM. LC-MS/MS was used to determine the composition of XHQDD and the composition of drug-containing

serum. The study results identified 14 prodrug components of XHQDD. Choline [45], sugiol [46], petroselinic acid [47], curdione [48], and kukoamine A [49] have been found to have anti-inflammatory effects, with some components also exhibiting inhibitory effects on the JAK/STAT pathway [50, 51]. Choline deficiency has been linked to cholestasis and abnormal liver function [52], but this can be corrected through choline supplementation. Additionally, choline, sugiol, curdione, and kukoamine A [53-55] have been shown to have protective effects against liver injury.

Cholestasis is an impairment in bile secretion flow due to intra- and extrahepatic causes. This study found that ANIT-induced cholestatic liver injury in rats exhibited a decrease in bile flow, suggesting the presence of cholestasis, which was ameliorated by XHQDD. Pathological staining revealed lipid-like deposits, nodular tissue hyperplasia, and inflammatory cell infiltration in the liver tissues of ANIT-treated rats, indicating concurrent hepatocellular damage with cholestasis. In contrast, XHQDD treatment mitigated this pathological damage.

ALP activity increases in all forms of cholestasis [56, 57]. The combined elevation of ALP and gamma-glutamyl transferase ($\gamma$-GT) can indicate obstructive or cholestatic liver disease, where bile is not properly transported from the liver due to bile duct obstruction [58, 59]. ALT and AST, predominantly found in the liver, are cytosolic and mitochondrial enzymes, respectively. They become elevated when hepatocellular damage occurs, releasing these enzymes into circulation [60]. Another feature of cholestatic liver disease is elevated serum BA levels [61]. Elevated serum levels of TBIL and DBIL serve as crucial markers for assessing the severity of liver injury [62, 63]. Our findings are consistent with previous studies that ANIT-induced hepatic injury in rats resulted in significantly elevated serum AST, ALT, $\gamma$-GT, ALP, TBA, TBIL, and DBIL levels, further suggesting the development of cholestasis. XHQDD treatment effectively mitigated these changes in a dose-dependent manner.

Cholestasis, a condition characterized by impaired bile production, leads to the accumulation of toxic bile constituents, such as bile salts. If left untreated, cholestasis can progress to liver fibrosis and cirrhosis, potentially resulting in liver failure [64, 65]. ANIT is a commonly used chemical in models of cholestasis and liver fibrosis. Consistent with previous studies [66], the present investigation revealed hepatic fibrosis manifestations in ANIT-treated rats, as demonstrated by Sirius red staining. Moreover, immunohistochemical analysis indicated increased expression of Col I and $\alpha$-SMA proteins. This trend was significantly ameliorated in the XHQDD and UDCA groups, with the XHQDD-H group exhibiting a comparable performance to the UDCA group.

Recent studies have demonstrated the significance of the JAK2/STAT3 signaling pathway in liver injury [67], and have indicated that downregulating this pathway reduces inflammation associated with liver injury [68]. The cascade initiates with the binding of ligands, predominantly cytokines like IL-6, to their respective cell surface receptors, such as the IL-6R/gp130 complex [69]. This binding event prompts the autophosphorylation of JAK2 associated with the intracellular domain of these receptors. Activated JAK2 subsequently phosphorylates specific tyrosine residues on the receptor, creating docking sites for STAT3. STAT3, upon recognizing and binding to these phosphorylated tyrosine residues, becomes a substrate for JAK2. This interaction leads to the phosphorylation of STAT3 at its Tyr705 residue, initiating its dimerization. Once dimerized, STAT3 translocates to the nucleus, where it binds to specific DNA response elements, inducing transcription of target genes involved in cell survival, proliferation, inflammation, and fibrosis, all of which are processes that are dysregulated in cholestatic liver injury [15, 70]. Our study discovered that the JAK2/STAT3 inflammatory pathway was activated in ANIT-induced cholestatic rats. In the liver, the expression of JAK2

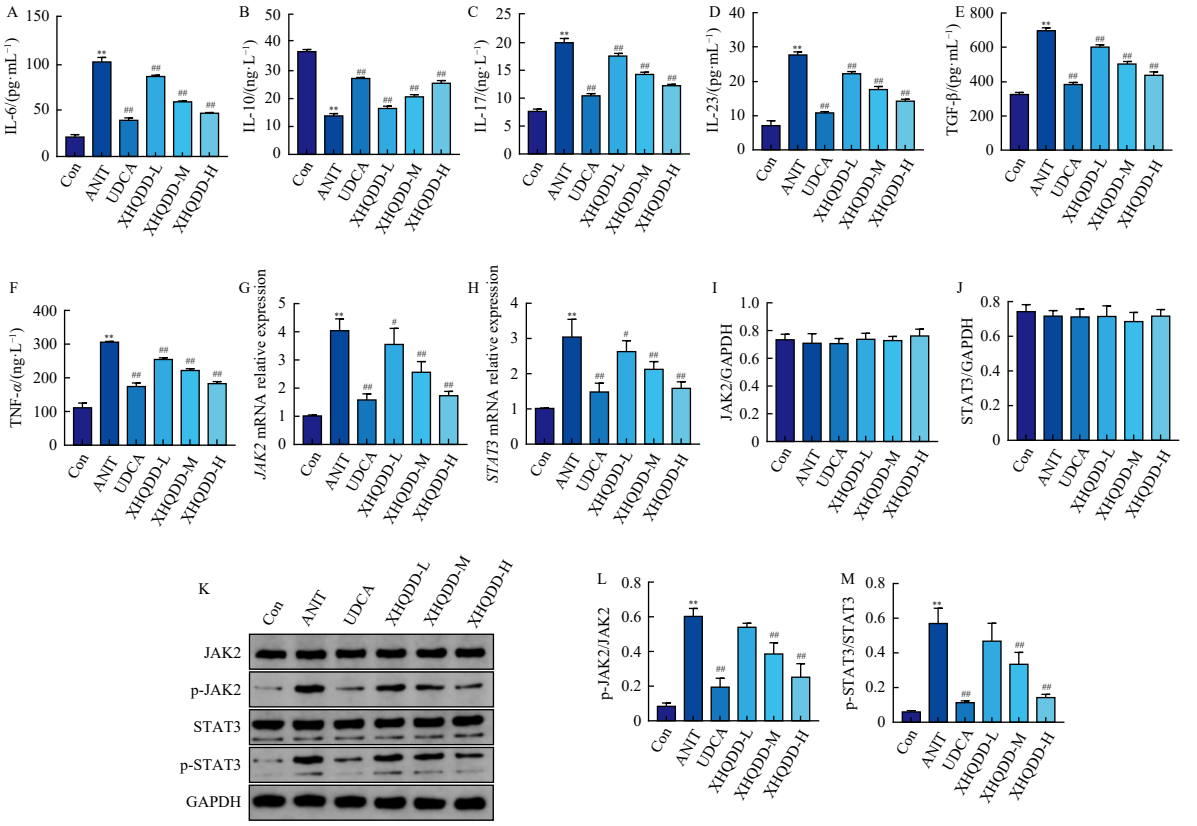


**Fig. 5** Expression of inflammatory factors and the JAK2/STAT3 pathway. (A) IL-6. (B) IL-10. (C) IL-17. (D) IL-23. (E) TGF-β. (F) TNF-α. (G) JAK2 mRNA expression. (H) STAT3 mRNA expression. (I) JAK2 protein expression. (J) STAT3 protein expression. (K) Protein bands. (L) p-JAK2 protein expression. (M) p-STAT3 protein expression. Data are shown as means ± SD ($n$ = 10). $^{**}P < 0.01$ *vs* Con group; $^{\#}P < 0.05$, $^{\#\#}P < 0.01$ *vs* ANIT group.

and STAT3 genes, along with phosphorylated proteins, was significantly elevated, and serum levels of inflammatory factors were markedly increased. XHQDD treatment led to reduced levels of inflammatory factors and substantial inhibition of the JAK2/STAT3 pathway. These findings suggest that XHQDD may mitigate cholestatic inflammatory injury by suppressing the JAK2/STAT3 pathway.

Clinical studies have shown that intrahepatic cholestasis is closely related to intestinal injury [71]. Cholestatic liver disease is characterized by dysbiosis of the intestinal flora and excess toxic hepatic BA [72]. The gut-liver axis theory proposes a close relationship between the gut and liver, mediated by BA, which plays a crucial role in linking the two organs. Disruption of BA transport and homeostasis in vivo contributes to the development of cholestatic disease and affects intestinal injury [73]. Inflammation is an important factor in the gut-liver axis [74]. Protein expression of the JAK2/STAT3 pathway in intestinal tissues was detected by qPCR, WB, and immunohistochemistry, and the results were found to be consistent with those shown in liver tissues. This suggests that XHQDD may exert its efficacy by inhibiting the JAK2/STAT3 pathway.

It has been shown that the accumulation of BAs in the liver in cholestatic diseases causes a complex inflammatory immune response [75, 76]. A key mechanism in this immune response involves Th17 and Treg cells [77]. Inflammatory factors upregulate RORγt, which induces Th17 phenotype and IL-17 production [78]. Recent studies have highlighted the role of IL-17 in liver injury [79], particularly in biliary atresia and primary biliary cirrhosis [80]. Elevated IL-17 levels exacerbate neutrophil recruitment and activation in the liver, perpetuating bile duct damage and cholestasis [81]. Conversely, Treg cells, characterized by the expression of the transcription factor Foxp3, act as suppressors of immune responses.

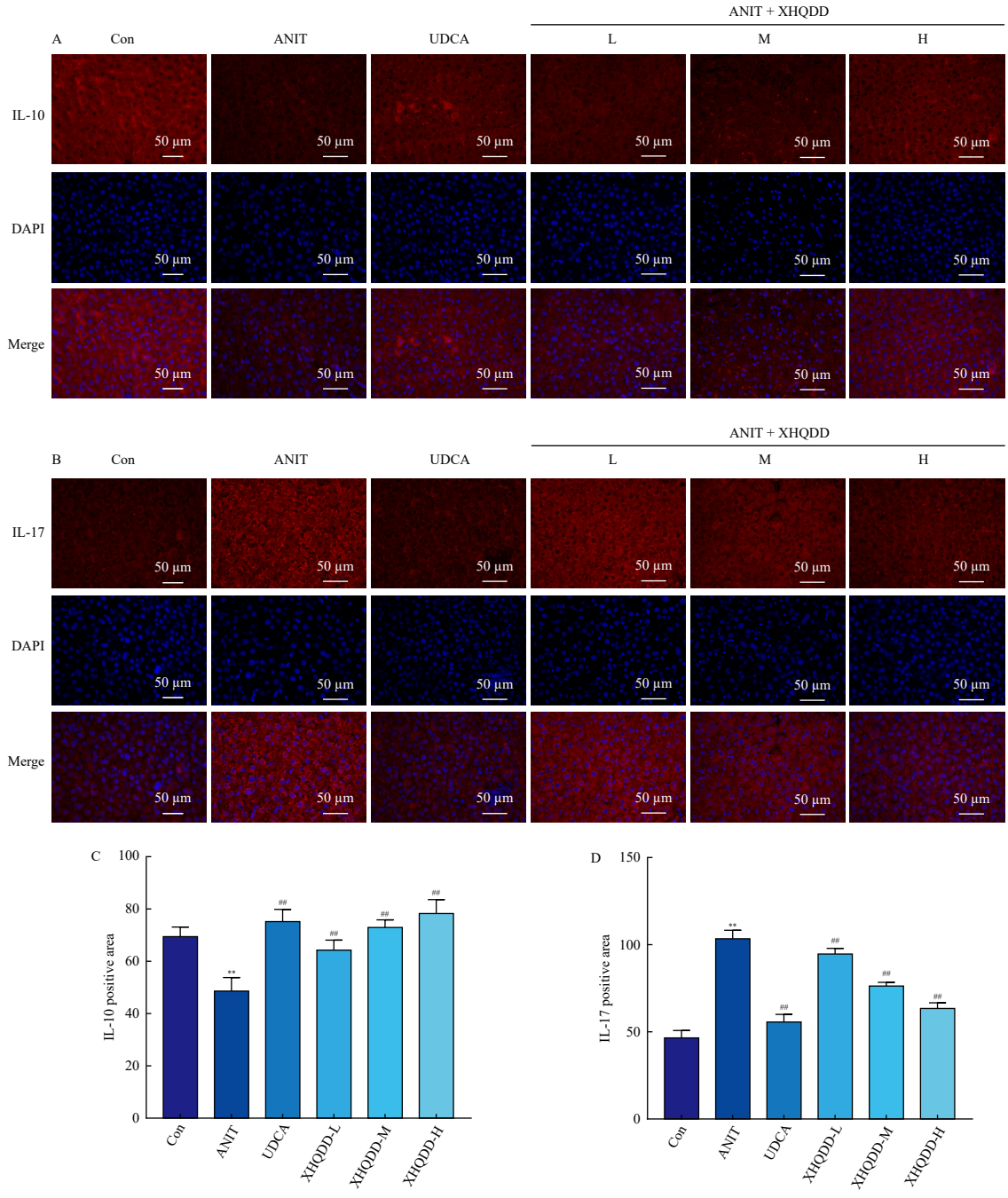


**Fig. 6** IL-10 and IL-17 protein expression. (A) Immunofluorescence graph of IL-10. (B) Immunofluorescence graph of IL-17. (C) IL-10 positive area. (D) IL-17 positive area. Data are shown as means ± SD ($n$ = 10). $^{**}P < 0.01$ *vs* Con group; $^{\#\#}P < 0.01$ *vs* ANIT group.

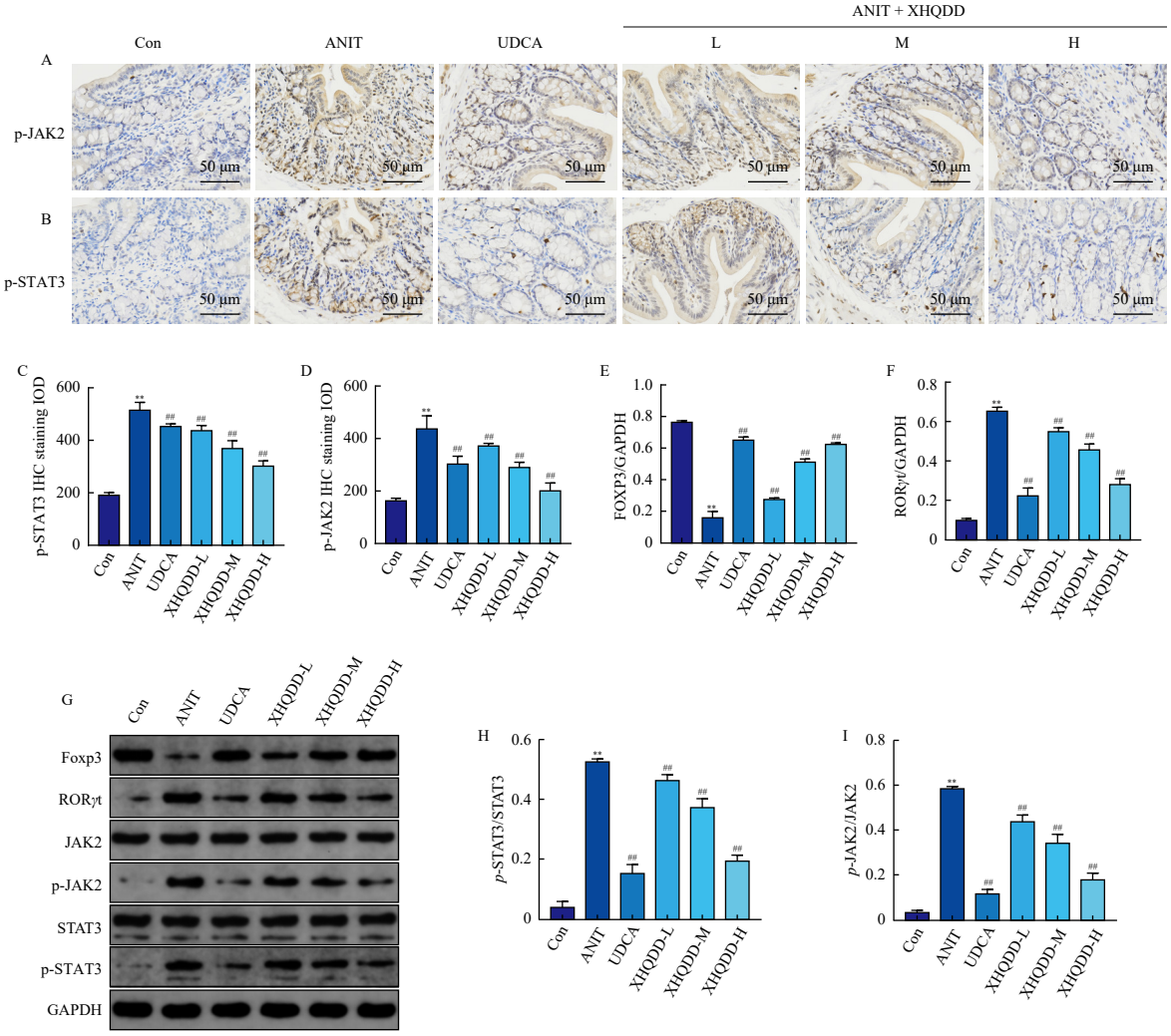


**Fig. 7** XHQDD suppresses the JAK2/STAT3 signalling pathway in colon tissue. (A–B) Representative images of p-JAK2 and p-STAT3 protein expression in colon tissues were obtained using IHC. (C–D) The results show the mean IOD of p-JAK2 and p-STAT3 proteins stained by IHC. (E–I) JAK2, p-JAK2, STAT3, p-STAT3, RORγt, and Foxp3 protein expressions. Data are shown as means ± SD ($n$ = 10). $^{**}P < 0.01$ *vs* Con group; $^{\#\#}P < 0.01$ *vs* ANIT group.

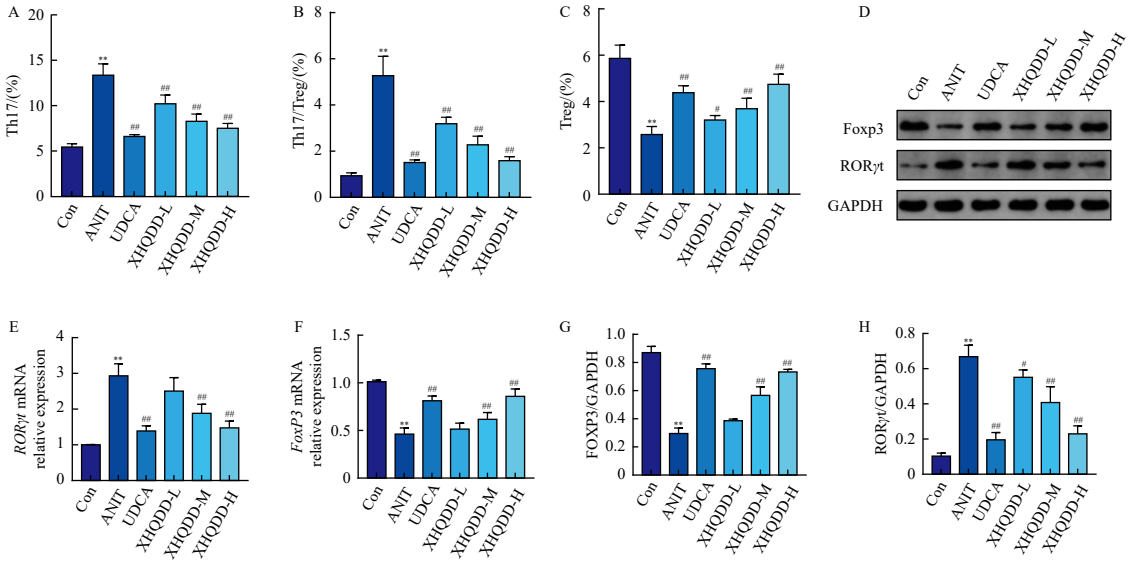


**Fig. 8** Flow analysis of Th17/Treg in liver tissue. (A)Percentage of Th17 cells. (B–C) Percentage of Treg cells. (D) RORγt and FOXP3 protein bands. (E) RORγt mRNA expression. (F) FOXP3 mRNA expression. (G) FOXP3 protein expression. (H) RORγt protein expression. Data are shown as means ± SD ($n$ = 10). $^{**}P < 0.01$ *vs* Con group; $^{\#}P < 0.05$; $^{\#\#}P < 0.01$ *vs* ANIT group.

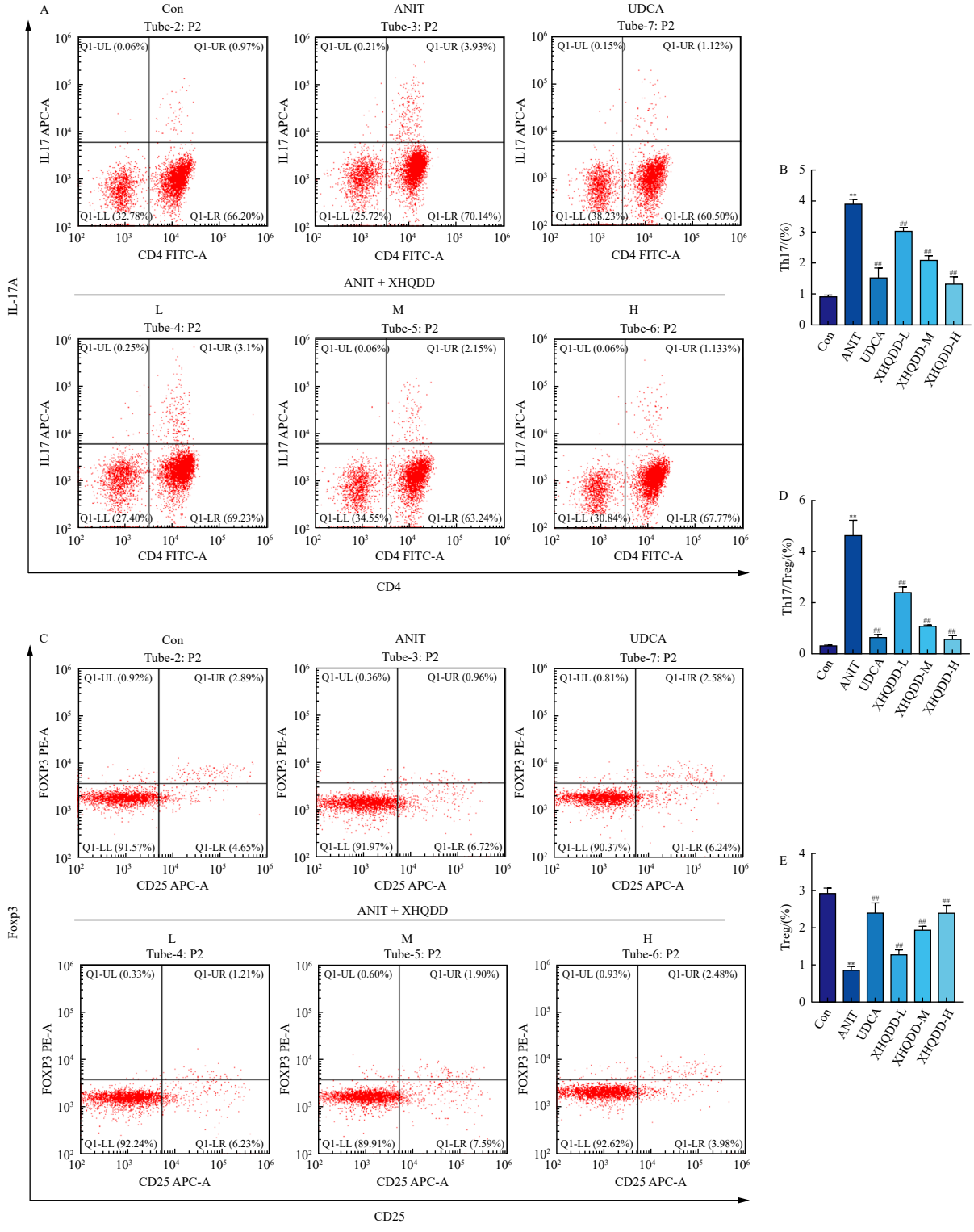


**Fig. 9** Serum Th17/Treg flow analysis. (A–B) Percentage of Th17 cells. (C) Th17/Treg ratio. (D–E) Percentage of Treg cells. Data are shown as means ± SD ($n$ = 10). $^{**}P$ < 0.01 *vs* Con group; $^{\#\#}P$ < 0.01 *vs* ANIT group.

They produce anti-inflammatory cytokines like IL-10 and TGF-β, while Treg cells alleviate liver injury depending on the secretion of IL-10 and TGF-β [63]. In cholestatic liver injury, the balance between Th17 and Treg cells is frequently disrupted. Studies have shown that, in conditions like primary biliary cholangitis (PBC), there's an increase in the Th17/Treg ratio, indicating a shift towards a more pro-inflammatory state [13, 82]. Notably, BAs themselves can influence this Th17/Treg balance [83]. However, in pathological cholestasis, the BA composition is altered, which might disrupt this protective shift towards Treg cell dominance [84].

Our study confirms this phenomenon. We assessed the Th17/Treg cell counts in the liver and serum of ANIT rats, revealing a disruption in Th17/Treg homeostasis in the presence of cholestasis. This imbalance was characterized by a significantly higher proportion of Th17 cells promoting inflammation and a markedly lower proportion of Treg cells. Additionally, the Th17 and Treg transcription factors RORγt and Foxp3 proteins exhibited corresponding changes. XHQDD was able to reverse this change and restore the Th17/Treg balance in a dose-dependent manner, with a more significant effect observed in the XHQDD-H

group compared to the XHQDD-L group.

The JAK2/STAT3 signaling pathway plays a critical role in influencing the Th17/Treg immune balance, a pivotal factor in the inflammatory environment of cholestatic liver injury [85]. Specifically, activation of the JAK2/STAT3 pathway promotes the secretion of pro-inflammatory cytokines, such as IL-17, from Th17 cells. This occurs when stimulation of the JAK2/STAT3 pathway leads to the translocation of STAT3 to the nucleus, which in turn upregulates the transcription of the *RORγt* gene [86], thereby enhancing Th17 cell proliferation and amplifying the pro-inflammatory response in cholestasis. Conversely, a hyperactivated JAK2/STAT3 pathway can impede the expression of FoxP3, a master regulator for Treg cells, diminishing the Treg population and their suppressive functions [87]. Furthermore, in cholestatic liver injury scenarios, the accumulation of BAs can further exacerbate the JAK2/STAT3 signaling. Elevated BAs have been shown to potentiate IL-6 production [88], a key activator of the JAK2/STAT3 pathway [89], which can accentuate the Th17/Treg imbalance by bolstering Th17 differentiation while suppressing Treg cell function [90].

Autophagy, a cellular process by which cells degrade and recycle damaged organelles and proteins, has been increasingly recognized as a key player in liver disease, and the activation of autophagy is protective against acute liver injury [91, 92]. In cholestatic liver injury, autophagy is induced as a protective response to counteract the hepatocellular damage caused by the accumulation of BAs. BAs can induce endoplasmic reticulum (ER) stress and mitochondrial damage, potentially resulting in cell death if left unaddressed. Autophagy is stimulated in an effort to eliminate these damaged organelles and alleviate the harmful effects of BAs [93, 94].

Furthermore, emerging evidence suggests that autophagy can modulate inflammatory responses in acute liver injury [95]. Autophagy regulates the release of pro-inflammatory cytokines, influencing the liver's immune milieu, with potential cascading effects on cholestatic liver disease progression [96]. The interaction between autophagy and cholestasis was not explored in depth in this study. Interestingly, autophagy was observed following XHQDD treatment in our study, as confirmed by TEM. Further validation of autophagy's protective role against cholestatic liver injury is warranted, necessitating additional studies. This provides a new therapeutic mechanism for XHQDD against cholestatic liver injury and points the way to the next step. The current study was limited by the lack of intervention with a JAK2/STAT3 pathway inhibitor. It is important to note that the herbal compound XHQDD has a multi-component and multi-target nature, and, therefore, the JAK2/STAT3 pathway may be just one of the mechanisms by which XHQDD exerts its effects in the treatment of cholestatic liver injury. Further research is required to identify the effective components of XHQDD for subsequent investigation.

## 5. Conclusion

This study presents compelling evidence demonstrating that the TCM formulation XHQDD can alleviate cholestatic liver injury. The findings indicate that XHQDD reverses disturbances in hepatic enzyme, bile acid, and bilirubin homeostasis while also inhibiting inflammatory factors through modulation of the JAK2/STAT3 signaling cascade. Additionally, XHQDD exhibits a dose-dependent efficacy in regulating the Th17/Treg cell imbalance. To our knowledge, this study represents the first comprehensive elucidation of the pharmacological mechanism of the clinically established TCM formulation XHQDD, examining it from molecular, cellular, and animal-based perspectives, as well as considering the influences on inflammation and immune phenotypes. These insights pave the way for a deeper understanding of the pharmacology of TCM formulations.

## Funding

This work was supported by the Natural Science Foundation of Hubei Province (No. 2022CFD020), the Postdoctoral Research Initiation Fund (No. 20211015KY19), and the Hubei Provincial Medical Young Top Talents [No. 2019(48)].

## Supporting Information

Supporting information for this study is available upon request *via* email to the corresponding authors.

## Declaration of Competing Interest

These authors have no conflict of interest to declare.

## References

1 Xu JJ, Xu F, Wang W, et al. Paeoniae Radix Rubra can enhance fatty acid β-oxidation and alleviate gut microbiota disorder in α-naphthyl isothiocyanate induced cholestatic model rats. *Front Pharmacol*. 2022;13(5):1002922. https://doi.org/10.3389/fphar.2022.1002922.
2 Colares JR, Hartmann RM, Schemitt EG, et al. Melatonin prevents oxidative stress, inflammatory activity, and DNA damage in cirrhotic rats. *World J Gastroenterol*. 2022;28(3):348-364. https://doi.org/10.3748/wjg.v28.i3.348.
3 Ferreira-Silva M, Faria-Silva C, Carvalheiro MC, et al. Quercetin liposomal nanoformulation for ischemia and reperfusion injury treatment. *Pharmaceutics*. 2022;14(1):.15513. https://doi.org/10.3390/pharmaceutics14010104.
4 Zollner G, Trauner M. Mechanisms of cholestasis. *Clin Liver Dis*. 2008;12(1):1-26,vii. https://doi.org/10.1016/j.cld.2007.11.010.
5 Amirneni S, Haep N, Gad MA, et al. Molecular overview of progressive familial intrahepatic cholestasis. *World J Gastroenterol*. 2020;26(47):7470-7484. https://doi.org/10.3748/wjg.v26.i47.7470.
6 Perez-Cuadrado-Robles E, Becq A, Rahmi G. Choosing the optimal stent in malignant extrahepatic biliary obstruction: What is the most pertinent outcome?. *Dig Endosc*. 2022;34(5):952-954. https://doi.org/10.1111/den.14332.
7 Xu J, Kausalya PJ, Van Hul N, et al. Protective functions of ZO-2/Tjp2 expressed in hepatocytes and cholangiocytes against liver injury and cholestasis. *Gastroenterology*. 2021;160(6):2103-2118. https://doi.org/10.1053/j.gastro.2021.01.027.
8 Chiang JY. Bile acid metabolism and signaling. *Compr Physiol*. 2013;3(3):1191-1212. https://doi.org/10.1002/cphy.c120023.
9 Li M, Cai SY, Boyer JL. Mechanisms of bile acid mediated inflammation in the liver. *Mol Aspects Med*. 2017;56:45-53. https://doi.org/10.1016/j.mam.2017.06.001.
10 Shi T, Malik A, Yang Vom Hofe A, et al. Farnesoid X receptor antagonizes macrophage-dependent licensing of effector T lymphocytes and progression of sclerosing cholangitis. *Sci Transl Med*. 2022;14(675):eabi4354. https://doi.org/10.1126/scitranslmed.abi4354.
11 Nguyen K, D'Mello C, Le T, et al. Regulatory T cells suppress sickness behaviour development without altering liver injury in cholestatic mice. *J Hepatol*. 2012;56(3):626-631. https://doi.org/10.1016/j.jhep.2011.09.014.
12 Zhong YM, Wu XR, Wang Q, et al. Changes in peripheral blood 25-hydroxyvitamin $D_3$, Th17 cells, and $CD4^+$ regulatory T cells and their clinical significance in patients with primary biliary cirrhosis. *Chin J Hepatol*. 2016;24(11):829-833. https://doi.org/10.3760/cma.j.issn.1007-3418.2016.11.007.
13 Cichoż-Lach H, Grywalska E, Michalak A, et al. Deviations in peripheral blood cell populations are associated with the stage of primary biliary cholangitis and presence of itching. *Arch Immunol Ther Exp (Warsz)*. 2018;66(6):443-452. https://doi.org/10.1007/s00005-018-0515-9.
14 Mulcahy V, Liaskou E, Martin JE, et al. Regulation of immune responses in primary biliary cholangitis: a transcriptomic analysis of peripheral immune cells. *Hepatol Commun*. 2023;7(4):265-274. https://doi.org/10.1097/HC9.0000000000000110.
15 Lee CH, Choi Y, Cho H, et al. Histone deacetylase 8 inhibition alleviates cholestatic liver injury and fibrosis. *Biochem Pharmacol*. 2021;183:114312. https://doi.org/10.1016/j.bcp.2020.114312.
16 Zhang C, Li S, Sun C, et al. Vitexin ameliorates glycochenodeoxycholate-induced hepatocyte injury through SIRT6 and JAK2/STAT3 pathways. *Iran J Basic Med Sci*. 2021;24(12):1717-1725. https://doi.org/10.22038/IJBMS.2021.59424.13196.
17 Zhao R, Dong R, Yang Y, et al. MicroRNA-155 modulates bile duct inflammation by targeting the suppressor of cytokine signaling 1 in biliary atresia. *Pediatr Res*. 2017;82(6):1007-1016. https://doi.org/10.1038/pr.2017.87.
18 Wu SY, Cui SC, Wang L, et al. 18β-Glycyrrhetinic acid protects against α-naphthylisothiocyanate-induced cholestasis through activation of the Sirt1/FXR signaling pathway. *Acta Pharmacol Sin*. 2018;39(12):1865-1873. https://doi.org/10.1038/s41401-018-0110-y.

19 Ferrell JM, Pathak P, Boehme S, et al. Deficiency of both farnesoid X receptor and takeda G protein-coupled receptor 5 exacerbated liver fibrosis in mice. *Hepatology*. 2019;70(3):955-970. https://doi.org/10.1002/hep.30513.

20 Fuchs CD, Paumgartner G, Mlitz V, et al. Colesevelam attenuates cholestatic liver and bile duct injury in *Mdr2*$^{-/-}$ mice by modulating composition, signalling and excretion of faecal bile acids. *Gut*. 2018;67(9):1683-1691. https://doi.org/10.1136/gutjnl-2017-314553.

21 Hirschfield GM, Mason A, Luketic V, et al. Efficacy of obeticholic acid in patients with primary biliary cirrhosis and inadequate response to ursodeoxycholic acid. *Gastroenterology*. 2015;148(4):751-761. e758. https://doi.org/10.1053/j.gastro.2014.12.005.

22 Jang E, Kim BJ, Lee KT, et al. A survey of therapeutic effects of *Artemisia capillaris* in liver diseases. *Evid Based Complement Alternat Med*. 2015;2015:728137. https://doi.org/10.1155/2015/728137.

23 Liu X, Zhao X. Scoparone attenuates hepatic stellate cell activation through inhibiting TGF-β/Smad signaling pathway. *Biomed Pharmacother*. 2017;93:57-61. https://doi.org/10.1016/j.biopha.2017.06.006.

24 Liu W, Tu Z, Liu J, et al. Therapeutic effect of Yinchenhao decoction on cholelithiasis *via* mucin in the gallbladder and intestine. *Fitoterapia*. 2024;172:105746. https://doi.org/10.1016/j.fitote.2023.105746.

25 Zeng M, Li M, Zhang L, et al. Different meridian tropism in three Chinese medicines: Tinglizi (Semen Lepidii Apetali), Yiyiren (Semen Coicis), Cheqianzi (Semen Plantaginis). *J Tradit Chin Med*. 2019;39(2):213-220. https://doi.org/10.19852/j.cnki.jtcm.2019.02.009.

26 Kim BH, Park KS, Chang IM. Elucidation of anti-inflammatory potencies of *Eucommia ulmoides* bark and *Plantago asiatica* seeds. *J Med Food*. 2009;12(4):764-769. https://doi.org/10.1089/jmf.2008.1239.

27 Yang PW, Xu PL, Cheng CS, et al. Integrating network pharmacology and experimental models to investigate the efficacy of QYHJ on pancreatic cancer. *J Ethnopharmacol*. 2022;297:115516. https://doi.org/10.1016/j.jep.2022.115516.

28 Pannee C, Chandhanee I, Wacharee L. Antiinflammatory effects of essential oil from the leaves of *Cinnamomum cassia* and cinnamaldehyde on lipopolysaccharide-stimulated J774A. 1 cells. *J Adv Pharm Technol Res*. 2014;5(4):164-170. https://doi.org/10.4103/2231-4040.143034.

29 Xie J, Wang YY, Li JX, et al. Effect and mechanism of *Poria cocos* polysaccharides on myocardial cell apoptosis in rats with myocardial ischemia-reperfusion injury by regulating Rho-ROCK signaling pathway. *China J Chin Mater Med*. 2023;48(23):6434-6441. https://doi.org/10.19540/j.cnki.cjcmm.20230816.401.

30 Huang DF, Xie MY, Yin JY, et al. Immunomodulatory activity of the seeds of *Plantago asiatica* L.. *J Ethnopharmacol*. 2009;124(3):493-498. https://doi.org/10.1016/j.jep.2009.05.017.

31 Zhang W, He J, Zheng D, et al. Immunomodulatory activity and its mechanisms of two polysaccharides from *Poria cocos*. *Molecules*. 2023;29(1):50. https://doi.org/10.3390/molecules29010050.

32 Zhimin C, Mingyue AO, Yujiao L, et al. Wuzi Yanzong prescription from traditional Chinese medicine for male infertility: a narrative review. *J Tradit Chin Med*. 2023;43(2):416-428. https://doi.org/10.19852/j.cnki.jtcm.20221214.001.

33 Li L. Clinical observation on 11 cases of acute jaundice hepatitis treated with Xiao-Huang-Qu-Dan decoction. *J Chengdu Coll Tradit Chin Med*. 1984;14(4):23-24.

34 Zhou HQ, Liu W, Wang J, et al. Paeoniflorin attenuates ANIT-induced cholestasis by inhibiting apoptosis *in vivo via* mitochondria-dependent pathway. *Biomed Pharmacother*. 2017;89(7):696-704. https://doi.org/10.1016/j.biopha.2017.02.084.

35 Wei X, Fan X, Feng Z, et al. Ethyl acetate extract of *Herpetospermum pedunculosum* alleviates α-naphthylisothiocyanate-induced cholestasis by activating the farnesoid x receptor and suppressing oxidative stress and inflammation in rats. *Phytomedicine*. 2020;76(4):153257. https://doi.org/10.1016/j.phymed.2020.153257.

36 Liu J, Liu J, Meng C, et al. Oleanolic acid alleviates ANIT-induced cholestatic liver injury by activating Fxr and Nrf2 pathways to ameliorate disordered bile acids homeostasis. *Phytomedicine*. 2022;102(12):154173. https://doi.org/10.1016/j.phymed.2022.154173.

37 Jia J, Feng L, Ye S, et al. Therapeutic effect of chinese herbal medicine gu-ben-hua-shi (AESS) formula on atopic dermatitis through regulation of yes-associated protein. *Front Pharmacol*. 2022;13(14):929580. https://doi.org/10.3389/fphar.2022.929580.

38 Wu P, Qiao L, Yu H, et al. Arbutin alleviates the liver injury of α-naphthylisothiocyanate-induced cholestasis through farnesoid X receptor activation. *Front Cell Dev Biol*. 2021;9(15):758632. https://doi.org/10.3389/fcell.2021.758632.

39 Khayat MT, Mohammad KA, Mohamed GA, et al. γ-Mangostin abrogates AINT-induced cholestatic liver injury: impact on Nrf2/NF-κB/NLRP3/Caspase-1/IL-1β/GSDMD signalling. *Life Sci*. 2023;322(13):121663. https://doi.org/10.1016/j.lfs.2023.121663.

40 Silva-Veiga FM, Miranda CS, Vasques-Monteiro IML, et al. Peroxisome proliferator-activated receptor-α activation and dipeptidyl peptidase-4 inhibition target dysbiosis to treat fatty liver in obese mice. *World J Gastroenterol*. 2022;28(17):1814-1829. https://doi.org/10.3748/wjg.v28.i17.1814.

41 Zhan X, Peng W, Wang Z, et al. Polysaccharides from garlic protect against liver injury in DSS-induced inflammatory Bowel disease of mice *via* suppressing pyroptosis and oxidative damage. *Oxid Med Cell Longev*. 2022;20(2):2042163. https://doi.org/10.1155/2022/2042163.

42 Zhang S, Zhong R, Tang S, et al. Baicalin alleviates short-term lincomycin-induced intestinal and liver injury and inflammation in infant mice. *Int J Mol Sci*. 2022;23(11):1542-1554. https://doi.org/10.3390/ijms23116072.

43 Wang Y, Shi K, Tu J, et al. Atractylenolide III ameliorates bile duct ligation-induced liver fibrosis by inhibiting the PI3K/AKT pathway and regulating glutamine metabolism. *Molecules*. 2023;28(14):546814. https://doi.org/10.3390/molecules28145504.

44 Zhou Y, Zhou Y, Li Y, et al. Targeted bile acid profiles reveal the liver injury amelioration of Da-Chai-Hu decoction against ANIT- and BDL-induced cholestasis. *Front Pharmacol*. 2022;13(2):959074. https://doi.org/10.3389/fphar.2022.959074.

45 Chen J, Vitetta L. Gut microbiota metabolites in NAFLD pathogenesis and therapeutic implications. *Int J Mol Sci*. 2020;21(15):13541. https://doi.org/10.3390/ijms21155214.

46 Bajpai VK, Sonwal S, Hwang SK, et al. Sugiol, a diterpenoid: therapeutic actions and molecular pathways involved. *Pharmacol Res*. 2021;163:105313. https://doi.org/10.1016/j.phrs.2020.105313.

47 Hajib A, El Harkaoui S, Choukri H, et al. Apiaceae family an important source of petroselinic fatty acid: abundance, biosynthesis, chemistry, and biological proprieties. *Biomolecules*. 2023;13(11):368-377. https://doi.org/10.3390/biom13111675.

48 Yang K, Wu B, Wei W, et al. Curdione ameliorates sepsis-induced lung injury by inhibiting platelet-mediated neutrophil extracellular trap formation. *Int Immunopharmacol*. 2023;118(7):110082. https://doi.org/10.1016/j.intimp.2023.110082.

49 Liu X, Wang M, Song Y, et al. Kukoamine A inhibits C-C motif chemokine receptor 5 to attenuate lipopolysaccharide-induced lung injury. *Drug Dev Res*. 2022;83(6):1455-1466. https://doi.org/10.1002/ddr.21975.

50 Wang F, Zhang X, Liu W, et al. Activated natural killer cell promotes nonalcoholic steatohepatitis through mediating JAK/STAT pathway. *Cell Mol Gastroenterol Hepatol*. 2022;13(1):257-274. https://doi.org/10.1016/j.jcmgh.2021.08.019.

51 Li Z, Hao E, Cao R, et al. Analysis on internal mechanism of zedoary turmeric in treatment of liver cancer based on pharmacodynamic substances and pharmacodynamic groups. *Chin Herb Med*. 2022;14(4):479-493. https://doi.org/10.1016/j.chmed.2022.06.007.

52 Kohjima M, Enjoji M, Yada R, et al. Pathophysiological analysis of primary biliary cirrhosis focusing on choline/phospholipid metabolism. *Liver Int*. 2015;35(3):1095-1102. https://doi.org/10.1111/liv.12526.

53 Li G, Zhou F, Chen Y, et al. Kukoamine A attenuates insulin resistance and fatty liver through downregulation of Srebp-1c. *Biomed Pharmacother*. 2017;89(15):536-543. https://doi.org/10.1016/j.biopha.2017.02.024.

54 Mehedint MG, Zeisel SH. Choline's role in maintaining liver function: new evidence for epigenetic mechanisms. *Curr Opin Clin Nutr Metab Care*. 2013;16(3):339-345. https://doi.org/10.1097/MCO.0b013e3283600d46.

55 Haraguchi H, Ishikawa H, Kubo I. Antioxidative action of diterpenoids from *Podocarpus nagi*. *Planta Med*. 1997;63(3):213-215. https://doi.org/10.1055/s-2006-957655.

56 Watafua M, Ejiofor JI, Musa A, et al. *Acacia sieberiana* (Fabaceae) attenuates paracetamol and bile duct ligation-induced hepatotoxicity *via* modulation of biochemical and oxidative stress biomarkers. *Front Pharmacol*. 2022;13(8):959661. https://doi.org/10.3389/fphar.2022.959661.

57 Lew LC, Hor YY, Jaafar MH, et al. Lactobacillus strains alleviated hyperlipidemia and liver steatosis in aging rats *via* activation of AMPK. *Int J Mol Sci*. 2020;21(16):425-436. https://doi.org/10.3390/ijms21165872.

58 De Silva NMG, Borges MC, Hingorani AD, et al. Liver function and risk of type 2 diabetes: bidirectional mendelian randomization study. *Diabetes*. 2019;68(8):1681-1691. https://doi.org/10.2337/db18-1048.

59 Gerussi A, Bernasconi DP, O'Donnell SE, et al. Measurement of gamma glutamyl transferase to determine risk of liver transplantation or death in patients with primary biliary cholangitis. *Clin Gastroenterol Hepatol*. 2021;19(8):1688-1697. e1614. https://doi.org/10.1016/j.cgh.2020.08.006.

60 Mathur D, Morgan M, McKenzie J, et al. Intrahepatic cholestasis of pregnancy: dilemma in diagnosis and management. *J Matern Fetal Neonatal Med*. 2022;35(25):8975-8981. https://doi.org/10.1080/14767058.2021.2008896.

61 Abrigo J, Olguín H, Gutierrez D, et al. Bile acids induce alterations in mitochondrial function in skeletal muscle fibers. *Antioxidants (Basel)*. 2022;11(9):574561. https://doi.org/10.3390/antiox11091706.

62 Hsu PW, Liao PC, Kao YH, et al. The mutation hotspots at UGT1A locus may be associated with Gilbert's syndrome affecting the Taiwanese population. *Int J Mol Sci*. 2022;23(20):487542. https://doi.org/10.3390/ijms232012709.

63 Zhang C, Jin H, Wang Y, et al. Critical role of OX40 in drug-induced acute liver injury. *Br J Pharmacol*. 2020;177(14):3183-3196. https://doi.org/10.1111/bph.15041.

64 Ghonem NS, Assis DN, Boyer JL. Fibrates and cholestasis. *Hepatology*. 2015;62(2):635-643. https://doi.org/10.1002/hep.27744.

65 Levy C, Manns M, Hirschfield G. New treatment paradigms in primary biliary cholangitis. *Clin Gastroenterol Hepatol*. 2023;21(8):2076-2087. https://doi.org/10.1016/j.cgh.2023.02.005.

66 Chang J, Lan T, Li C, et al. Activation of Slit2-Robo1 signaling promotes liver fibrosis. *J Hepatol*. 2015;63(6):1413-1420. https://doi.org/10.1016/j.jhep.2015.07.033.

67 He X, Kang K, Pan D, et al. FTY720 attenuates APAP-induced liver injury *via* the JAK2/STAT3 signaling pathway. *Int J Mol Med*. 2022;49(5):789-799. https://doi.org/10.3892/ijmm.2022.5123.

68 Chen Y, Hou C, Yang N, et al. Regulatory effect of JAK2/STAT3 on the immune function of endotoxin-tolerant dendritic cells and its involvement in acute liver failure. *J Clin Transl Hepatol*. 2022;10(5):879-890. https://doi.org/10.14218/JCTH.2021.00175.

69 O'Shea JJ, Schwartz DM, Villarino AV, et al. The JAK-STAT pathway: impact on human disease and therapeutic intervention. *Annu Rev Med*. 2015;66(5):311-328. https://doi.org/10.1146/annurev-med-051113-024537.

70 Piao X, Sui X, Liu B, et al. Picroside II improves severe acute pancreatitis-induced hepatocellular injury in rats by affecting JAK2/STAT3 phosphorylation signaling. *Biomed Res Int*. 2021;20(12):9945149. https://doi.org/10.1155/2021/9945149.

71 Chen Z, Wu Y, Wang B, et al. Intrahepatic cholestasis induced by α-

naphthylisothiocyanate can cause gut-liver axis disorders. *Environ Toxicol Pharmacol*. 2021;86(16):103672. https://doi.org/10.1016/j.etap.2021.103672.
72 Liu Y, Chen K, Li F, et al. Probiotic *Lactobacillus rhamnosus* GG prevents liver fibrosis through inhibiting hepatic bile acid synthesis and enhancing bile acid excretion in mice. *Hepatology*. 2020;71(6):2050-2066. https://doi.org/10.1002/hep.30975.
73 Isaacs-Ten A, Echeandia M, Moreno-Gonzalez M, et al. Intestinal microbiome-macrophage crosstalk contributes to cholestatic liver disease by promoting intestinal permeability in mice. *Hepatology*. 2020;72(6):2090-2108. https://doi.org/10.1002/hep.31228.
74 Sun J, Zhang J, Wang X, et al. Gut-liver crosstalk in sepsis-induced liver injury. *Crit Care*. 2020;24(1):614. https://doi.org/10.1186/s13054-020-03327-1.
75 Bokemeyer A, Lenze F, Stoica V, et al. Digital single-operator video cholangioscopy improves endoscopic management in patients with primary sclerosing cholangitis-a retrospective observational study. *World J Gastroenterol*. 2022;28(20):2201-2213. https://doi.org/10.3748/wjg.v28.i20.2201.
76 Li M, Zhang X, Lu Y, et al. The nuclear translocation of transketolase inhibits the farnesoid receptor expression by promoting the binding of HDAC3 to FXR promoter in hepatocellular carcinoma cell lines. *Cell Death Dis*. 2020;11(1):31. https://doi.org/10.1038/s41419-020-2225-6.
77 Zeng L, Yang T, Yang K, et al. Efficacy and safety of curcumin and *Curcuma longa* extract in the treatment of arthritis: a systematic review and meta-analysis of randomized controlled trial. *Front Immunol*. 2022;13:891822. https://doi.org/10.3389/fimmu.2022.891822.
78 Tsiogkas SG, Mavropoulos A, Dardiotis E, et al. A sharp decrease of Th17, $CXCR3^+$-Th17, and Th17.1 in peripheral blood is associated with an early anti-IL-17-mediated clinical remission in psoriasis. *Clin Exp Immunol*. 2022;210(1):79-89. https://doi.org/10.1093/cei/uxac069.
79 Vujovic A, Isakovic AM, Misirlic-Dencic S, et al. IL-23/IL-17 axis in chronic hepatitis C and non-alcoholic steatohepatitis-new insight into immunohepatotoxicity of different chronic liver diseases. *Int J Mol Sci*. 2023;24(15):685-694. https://doi.org/10.3390/ijms241512483.
80 Jia H, Chen J, Zhang X, et al. IL-17A produced by invariant natural killer T cells and $CD3^+CD56^+$ αGalcer-CD1d tetramer–T cells promote liver fibrosis in patients with primary biliary cholangitis. *J Leukoc Biol*. 2022;112(5):1079-1087. https://doi.org/10.1002/JLB.2A0622-586RRRR.
81 Trivedi PJ, Adams DH. Chemokines and chemokine receptors as therapeutic targets in inflammatory Bowel disease; pitfalls and promise. *J Crohns Colitis*. 2018;12(12):1508. https://doi.org/10.1093/ecco-jcc/jjy130.
82 Hao LR, Li XF, Gao C, et al. Th17/Treg cell level and clinical characteristics of peripheral blood of patients with Sjogren's syndrome complicated with primary biliary cirrhosis. *Medicine (Baltimore)*. 2019;98(24):e15952. https://doi.org/10.1097/MD.0000000000015952.
83 Liu J, Fei Y, Zhou T, et al. Bile acids impair vaccine response in children with biliary atresia. *Front Immunol*. 2021;12(3):642546. https://doi.org/10.3389/fimmu.2021.642546.
84 Sun M, Wu W, Liu Z, et al. Microbiota metabolite short chain fatty acids, GPCR, and inflammatory bowel diseases. *J Gastroenterol*. 2017;52(1):1-8. https://doi.org/10.1007/s00535-016-1242-9.
85 Yang M, Zhang Q, Taha R, et al. Polysaccharide from *Atractylodes macrocephala* Koidz. ameliorates DSS-induced colitis in mice by regulating the Th17/Treg cell balance. *Front Immunol*. 2022;13(6):1021695. https://doi.org/10.3389/fimmu.2022.1021695.
86 Zhao Y, Luan H, Jiang H, et al. Gegen Qinlian decoction relieved DSS-induced ulcerative colitis in mice by modulating Th17/Treg cell homeostasis *via* suppressing IL-6/JAK2/STAT3 signaling. *Phytomedicine*. 2021;84(7):153519. https://doi.org/10.1016/j.phymed.2021.153519.
87 Jin C, Gao BB, Zhou WJ, et al. Hydroxychloroquine attenuates autoimmune hepatitis by suppressing the interaction of GRK2 with PI3K in T lymphocytes. *Front Pharmacol*. 2022;13(12):972397. https://doi.org/10.3389/fphar.2022.972397.
88 Nazmy EA, Helal MG, Said E. Nifuroxazide mitigates cholestatic liver injury by synergistic inhibition of Il-6/β-catenin signaling and enhancement of BSEP and $MDRP_2$ expression. *Int Immunopharmacol*. 2021;99(5):107931. https://doi.org/10.1016/j.intimp.2021.107931.
89 Zhang M, Wu W, Huang C, et al. Shuxie-1 decoction alleviated CUMS -induced liver injury *via* IL-6/JAK2/STAT3 signaling. *Front Pharmacol*. 2022;13(3):848355. https://doi.org/10.3389/fphar.2022.848355.
90 Jie XL, Luo ZR, Yu J, et al. Pi-Pa-Run-Fei-Tang alleviates lung injury by modulating IL-6/JAK2/STAT3/IL-17 and PI3K/AKT/NF-κB signaling pathway and balancing Th17 and Treg in murine model of OVA-induced asthma. *J Ethnopharmacol*. 2023;317(12):116719. https://doi.org/10.1016/j.jep.2023.116719.
91 Hu J, Ying H, Zheng Y, et al. Alanyl-glutamine protects against lipopolysaccharide-induced liver injury in mice *via* alleviating oxidative stress, inhibiting inflammation, and regulating autophagy. *Antioxidants (Basel)*. 2022;11(6):3214-3225. https://doi.org/10.3390/antiox11061070.
92 Feng L, Chen Y, Xu K, et al. Cholesterol-induced leucine aminopeptidase 3 (LAP3) upregulation inhibits cell autophagy in pathogenesis of NAFLD. *Aging (Albany NY)*. 2022;14(7):3259-3275. https://doi.org/10.18632/aging.204011.
93 Ruart M, Chavarria L, Campreciós G, et al. Impaired endothelial autophagy promotes liver fibrosis by aggravating the oxidative stress response during acute liver injury. *J Hepatol*. 2019;70(3):458-469. https://doi.org/10.1016/j.jhep.2018.10.015.
94 Gao J, Wei B, de Assuncao TM, et al. Hepatic stellate cell autophagy inhibits extracellular vesicle release to attenuate liver fibrosis. *J Hepatol*. 2020;73(5):1144-1154. https://doi.org/10.1016/j.jhep.2020.04.044.
95 Xu J, Zhao X, Jiang X, et al. Tubastatin A improves post-resuscitation myocardial dysfunction by inhibiting NLRP3-mediated pyroptosis through enhancing transcription factor EB signaling. *J Am Heart Assoc*. 2022;11(7):e024205. https://doi.org/10.1161/JAHA.121.024205.
96 Deretic V. Autophagy in inflammation, infection, and immunometabolism. *Immunity*. 2021;54(3):437-453. https://doi.org/10.1016/j.immuni.2021.01.018.